Vector Control Strategy of a T-type Three-level Converter Driving a Switched Reluctance Motor*

Mingyao Ma, Zhuangzhi Wang, Qingqing Yang, Shuying Yang and Xing Zhang*

(National and Local Joint Engineering Laboratory of Renewable Energy Access to Grid Technology, Hefei University of Technology, Hefei 230009, China)

Abstract: A novel 12 voltage vector control strategy for switched reluctance motors (SRM) with a T-type three-level converter is proposed in this study. Based on a causal analysis of torque ripple under the control of conventional six voltage vectors, six new voltage vectors are added for further reduction of torque ripple. An optimized control rule is adopted based on the division method of the 12 new voltage vectors. A zero-voltage vector is used to adjust the duration of the 12 voltage vectors, the time of which is varied at different parts of the vector sectors according to the torque error. In addition, the windings are connected in a delta configuration, therefore, the number of connections between the converter and SRM is reduced. Finally, the results of MATLAB/Simulink and RT-LAB are presented to verify the validity of the proposed scheme.

Keywords: Switched reluctance motor (SRM), T-type three-level converter, vector control

1 Introduction

With the growing environmental and energy crisis, electric vehicles are receiving an increasing amount of attention. Switched reluctance motors (SRMs) are strong candidates for electric vehicle drive systems, owing to their simple and robust structure, low cost, and high fault tolerance ability. However, the double salient pole structure and highly nonlinear inductance of SRMs result in a large torque ripple. To reduce the torque ripple, researchers primarily focus on two areas: an optimized structural design for SRMs, and a suitable control strategy.

Researchers have presented several control strategies to reduce the torque ripple. In Ref. [1], the author pointed out that the existence of a torque dip between two subsequent phases dictates the existence of torque ripples. A commutation angle, θ_c, is defined, at which two adjacent phases can produce the same torque for the same current. Based on the defined θ_c, specific current references for commutation are designed, which can theoretically eliminate the torque ripple due to the torque dip. In Ref. [2], a novel strategy of torque prediction based on direct instantaneous torque control (DITC) is proposed, which allows complete elimination of the inherent torque ripple encountered during phase commutation, without the use of offline-calculated current or flux profiles. An adjustable flux reference based on direct torque control (DTC) is used to minimize the torque ripple of SRMs in Ref. [3], in which a flux linkage closed-loop control is used to replace the original opening-loop control in the conventional DTC system in order to optimize the flux linkage during the commutation, and produce better performance than the conventional DTC method. In Ref. [4], a new DTC method that ignores the flux loop to obtain a more flexible selection of voltage vectors was proposed, which subsequently reduces the torque ripple. In Ref. [5], a DTC strategy for an induction machine with three level NPC converters was proposed for fault tolerance. The developed strategy was optimized by reducing the number of sectors in order to decrease the insulated-gate bipolar transistor's switching frequency. DTC directly controls the torque by selecting a suitable voltage vector to regulate the magnitude and rotational direction of the flux linkage. However, the torque ripple is still high during commutation, and the conventional DTC method does not take the commutation period into account. In Ref. [6], a three-phase full-bridge converter was used to drive the SRM, and a specially designed strategy was proposed to guarantee the torque performance. One obvious advantage is that the cost of its drive system is less than the conventional SRM drive system, owing to the lack of integrated modules for the asymmetric half-bridge converter (AHB). However, the three-phase full-bridge converter can only provide six voltage vectors, which is not sufficient to deal with the

* Corresponding Author, Email: miyama@hfut.edu.cn
* Supported by the National Natural Science Foundation of China (51977054).
Digital Object Identifier: 10.23919/CJEE.2019.000023

torque ripple problem during torque commutation when the conventional DTC method is used with the three-phase full-bridge converter to drive the SRM.

In this study, a novel 12 voltage vector control strategy with a T-type three-level converter is proposed to solve the high torque ripple problem in the conventional six voltage vector DTC method. First, six new voltage vectors are added to the original six voltage vectors by the middle bridge of the T-type three-level converter. The new voltage vectors are selected at the torque commutation area to reduce the torque ripple. Further, the causes of torque ripple with the conventional six voltage vectors are analyzed. Subsequently, a zero-voltage vector is used to adjust the duration of the 12 vectors, while the time is varied at different parts of the vector sectors. Finally, the results of the MATLAB/Simulink and RT-LAB analyses are presented to verify the effectiveness of the proposed scheme.

2 Topology of the SRM drive and its related DTC control method

DTC is usually adopted in SRMs with an asymmetric half-bridge converter topology [7-10]. There are some differences observed when DTC is adopted for the T-type three-level converter topology. These differences are comprehensively explained in the following sections.

2.1 Three-level topology of SRM drive

As shown in Fig. 1, a T-type three-level converter is used to drive a three-phase, 12/8 pole SRM. Owing to the delta connected windings, the phase voltages of the windings are equal to the line voltages of the converter. Each winding voltage can be $2U_{dc}$, U_{dc}, 0, $-U_{dc}$, and $-2U_{dc}$, as represented by $S = 2, 1, 0, -1$, and -2, respectively.

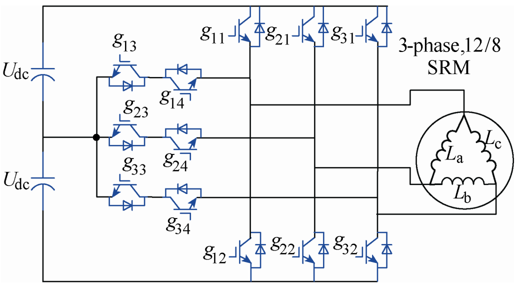

Fig. 1 T-type three-level converter

In the case of Phase A, for example, if g_{11} and g_{22} are both turned on, and the remaining 10 switches are turned off, the voltage of the winding L_a is $2U_{dc}$. The winding L_a is excited at voltage U_{dc}, only when g_{13}, g_{14}, and g_{22}, or only g_{11}, g_{23}, and g_{24} are turned on. Similarly, with only g_{13}, g_{14}, and g_{21}, or only g_{12}, g_{23}, and g_{24} turned on, the voltage is $-U_{dc}$. In the following three cases where only g_{11} and g_{21} are turned on, only g_{12} and g_{22} are turned on, or only g_{13}, g_{14}, g_{23} and g_{24} are turned on, the voltage is zero. Finally, when only g_{12} and g_{21} are turned on, the voltage of the winding L_a is $-2U_{dc}$.

2.2 Working principle of 12 voltage vectors

The conventional six voltage vectors are usually adopted in a two-level converter [11]. The T-type three-level converter has 27 switching states. We chose 12 effective voltage vectors and one zero-voltage vector from those 27 switching states to drive the SRM, where v_n (S_a, S_b and S_c) is the voltage vector by state of each winding voltage at L_a, L_b and L_c, respectively ("2" denotes $2U_{dc}$, "1" denotes U_{dc}, "0" denotes 0, "−1" denotes $-U_{dc}$, and "−2" denotes $-2U_{dc}$), as shown in Fig. 2. The area of the space vector is divided into 12 sectors, which are named by N_1 to N_{12} in the counterclockwise direction. According to the amplitude, those 12 voltage vectors can be divided into two parts: vectors 1, 3, 5, 7, 9 and 11 with an amplitude of $2\sqrt{3}\,U_{dc}$, and vectors 2, 4, 6, 8, 10 and 12 with an amplitude of $3U_{dc}$.

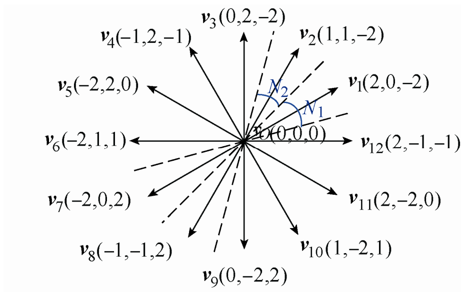

Fig. 2 Voltage vector sectors

For example, when the flux linkage vector rotates in the area of N_1, $\boldsymbol{v}_2$, $\boldsymbol{v}_3$, $\boldsymbol{v}_5$ and $\boldsymbol{v}_6$ can be selected to increase the torque. The reason for not selecting $\boldsymbol{v}_4$ is that it is perpendicular to $\boldsymbol{v}_1$, and perpendicular voltage vectors have no effect on torque. Further, according to the requirement of the flux linkage, $\boldsymbol{v}_2$ and $\boldsymbol{v}_3$ or $\boldsymbol{v}_5$ and $\boldsymbol{v}_6$ can be selected to increase or decrease the flux linkage, respectively. Similarly, $\boldsymbol{v}_{12}$, $\boldsymbol{v}_{11}$, $\boldsymbol{v}_9$ and $\boldsymbol{v}_8$ are selected to decrease the torque, and according to the flux linkage error, they are also divided into two parts. Tab. 2 shows the detailed situation at sector N_1, where the symbols ↑ and ↓ represent the command to increase or decrease the flux or torque, respectively.

As we can see in Tab. 1, there are two candidates for each torque and flux linkage state. According the DTC method, both can meet the requirements of the torque and flux linkage, and when only the vectors with odd subscripts are selected, the control strategy will be same as that of the conventional DTC method. The complete vector selection table is presented in Tab. 2. Based on the conventional vector selection method, the causes of torque ripple with the conventional six voltage vectors are analyzed.

Tab. 1 Vector selecting from 12 voltage vectors at sector N_1

	The change in torque and flux linkage			
	T↑ ψ↑	T↑ ψ↓	T↓ ψ↑	T↓ ψ↓
Voltage vector	$\boldsymbol{v}_3$	$\boldsymbol{v}_5$	$\boldsymbol{v}_{11}$	$\boldsymbol{v}_9$
	$\boldsymbol{v}_2$	$\boldsymbol{v}_6$	$\boldsymbol{v}_{12}$	$\boldsymbol{v}_8$

2.3 Analysis of torque ripple in conventional DTC

Based on the vector selection table of the conventional DTC theory shown in Tab. 2, a MATLAB/Simulink model is constructed with a 2-D look-up table. The reference speed is 500 r/min, the reference torque is 60 N·m, and the reference flux linkage is 0.38 Wb. The simulation results are shown in Fig. 3, and include the total torque, the three-phase torques, and the three-phase currents.

Tab. 2 Vector selecting from six odd subscript vectors based on conventional DTC theory

	The change in torque and flux linkage			
	T↑ ψ↑	T↑ ψ↓	T↓ ψ↑	T↓ ψ↓
N_1	$\boldsymbol{v}_3$	$\boldsymbol{v}_5$	$\boldsymbol{v}_{11}$	$\boldsymbol{v}_9$
N_2	$\boldsymbol{v}_3$	$\boldsymbol{v}_7$	$\boldsymbol{v}_1$	$\boldsymbol{v}_9$
N_3	$\boldsymbol{v}_5$	$\boldsymbol{v}_7$	$\boldsymbol{v}_1$	$\boldsymbol{v}_{11}$
N_4	$\boldsymbol{v}_5$	$\boldsymbol{v}_9$	$\boldsymbol{v}_3$	$\boldsymbol{v}_{11}$
N_5	$\boldsymbol{v}_7$	$\boldsymbol{v}_9$	$\boldsymbol{v}_3$	$\boldsymbol{v}_1$
N_6	$\boldsymbol{v}_7$	$\boldsymbol{v}_{11}$	$\boldsymbol{v}_5$	$\boldsymbol{v}_1$
N_7	$\boldsymbol{v}_9$	$\boldsymbol{v}_{11}$	$\boldsymbol{v}_5$	$\boldsymbol{v}_3$
N_8	$\boldsymbol{v}_9$	$\boldsymbol{v}_1$	$\boldsymbol{v}_7$	$\boldsymbol{v}_3$
N_9	$\boldsymbol{v}_{11}$	$\boldsymbol{v}_1$	$\boldsymbol{v}_7$	$\boldsymbol{v}_5$
N_{10}	$\boldsymbol{v}_{11}$	$\boldsymbol{v}_3$	$\boldsymbol{v}_9$	$\boldsymbol{v}_5$
N_{11}	$\boldsymbol{v}_1$	$\boldsymbol{v}_3$	$\boldsymbol{v}_9$	$\boldsymbol{v}_7$
N_{12}	$\boldsymbol{v}_1$	$\boldsymbol{v}_5$	$\boldsymbol{v}_{11}$	$\boldsymbol{v}_7$

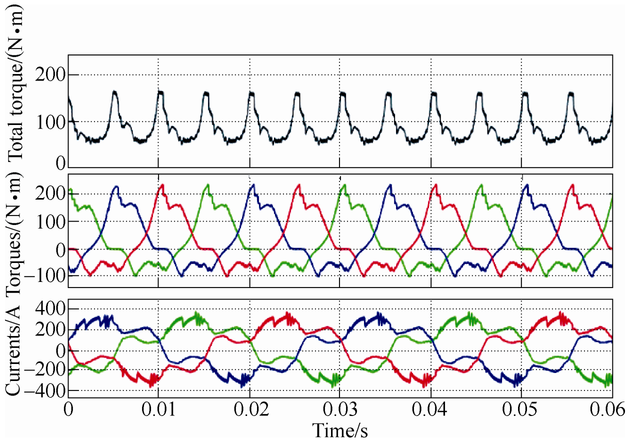

Fig. 3 Simulation results of six odd subscript vectors based on conventional DTC theory at 500 r/min

From the total torque and three-phase torques waveforms, a large torque ripple appears in the torque commutation zones. In these commutation zones, the torque generated by the outgoing phase declines, owing to the existence of negative torque there, the incoming phase has to generate positive torque in time. However, due to non-linear inductance in SRMs, the speed of the positive torque increases at a faster than that required by the negative torque, even if the negative continues to decrease. These observations lead to the large torque ripple in the commutation zones.

3 SRM drive system and control strategy

The SRM drive system proposed in this study is shown in Fig. 4. The control strategy normally used in AC or PM motors, which are also driven by conventional three-phase converters, cannot be directly employed for SRMs [12-15]. Additionally, the DTC method for the AHB driving the SRM drive system has to be modified to suit the T-type three-level converter. The control system in Fig. 4 is composed of a preprocessing part, a calculation part, and a T-type three-level converter. The specific components of each part are discussed in the following sections.

3.1 Preprocessing part

The preprocessing part includes a flux and torque calculation portion, and a sector determination portion. Owing to the highly nonlinear flux characteristics, it is difficult to accurately calculate the flux with the use of equations. In this study, as shown in Fig. 5a, a 2-D look-up table is adopted to provide instantaneous flux values according to the current and position

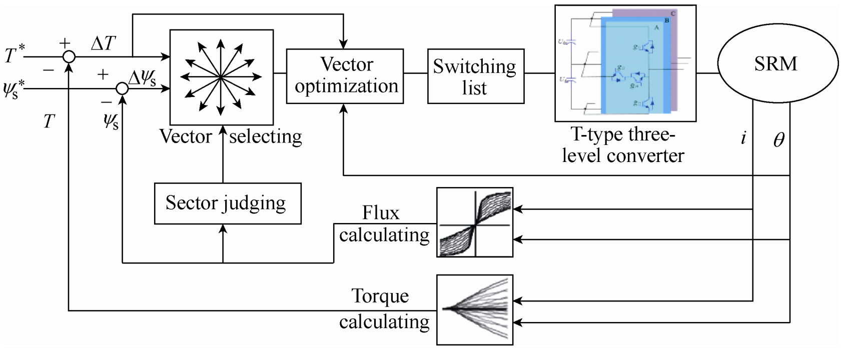

Fig. 4 Block diagram of the SRM drive system

information. Similarly, the instantaneous torque is provided by the 2-D look-up table depicted in Fig. 5b.

To obtain the amplitude and phase angle of the flux linkage, ψ_α and ψ_β are calculated using the reference frame conversion from a three-phase stationary reference frame to a two-phase stationary reference frame (3 s/2 s) as given by

$$\begin{cases} \psi_\alpha = \dfrac{2}{3}\left(\psi_a - \psi_b \cos 60^\circ - \psi_c \cos 60^\circ\right) \\ \psi_\beta = \dfrac{2}{3}\left(\psi_b \sin 60^\circ - \psi_c \sin 60^\circ\right) \end{cases} \tag{1}$$

where, ψ_a, ψ_b, and ψ_c are the three-phase flux linkages from the flux calculating portion.

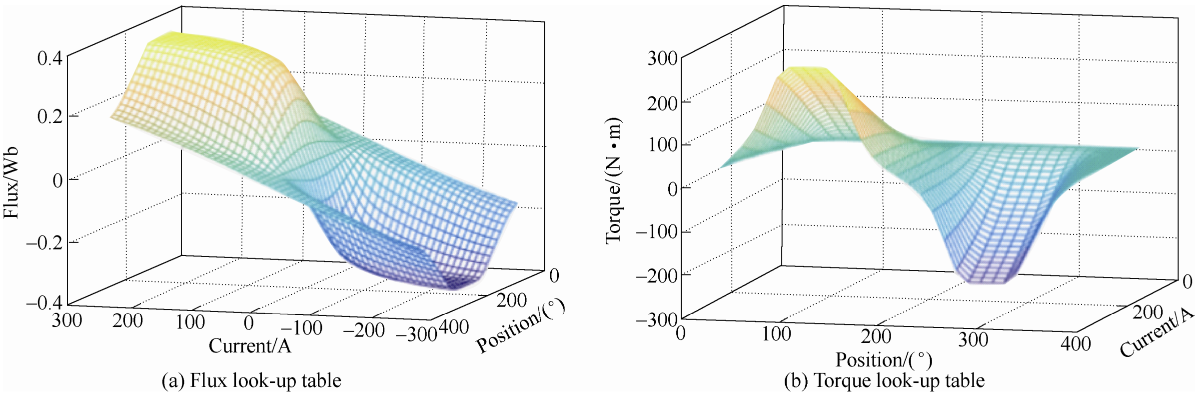

Fig. 5 Flux and torque look-up tables

The amplitude and phase angle of the flux linkage are given by

$$\begin{cases} |\psi_s| = \sqrt{\psi_\alpha^2 + \psi_\beta^2} \\ \gamma = \arctan\left(\dfrac{\psi_\beta}{\psi_\alpha}\right) \end{cases} \tag{2}$$

where ψ_s is the amplitude, and γ is the phase angle of the flux linkage.

According to the phase angle of the flux linkage and the voltage vector sector division method shown in Fig. 2, the sector judging portion can output the sector numbers where the current flux linkage vector is located.

3.2 Calculating part

The calculating part includes a vector selection portion, a vector optimization portion, and a switching list. Based on the causal analysis of torque ripple in conventional DTC, a new vector selection method is proposed, as presented in Tab. 3. The selection method is unchanged in the odd zones: N_1, N_3, N_5, N_7, N_9 and N_{11}. However, in the even zones N_2, N_4, N_6, N_8, N_{10} and N_{12}, the vectors with even subscripts replace the vectors with the odd subscripts.

With the new vectors in the even zones, the negative torque will decrease more quickly in order to meet the increasing speed of the positive torque in the torque commutation zones, such that the torque ripple will be reduced.

Owing to the amplitude difference between the odd and even subscript voltage vectors, the duration of the odd subscript voltage vectors has to be multiplied by a gain of 0.866. However, the torque ripple will still be high when only the 12 effective vectors are applied. In this study, the zero-voltage vector $\boldsymbol{v}_0$, is used to slow down the changing speed of the torque. Additionally, the duration of $\boldsymbol{v}_0$ is determined by the

Tab. 3 Vector selecting from 12 vectors based on the proposed method

	The change in torque and flux linkage			
	$T\uparrow\ \psi\uparrow$	$T\uparrow\ \psi\downarrow$	$T\downarrow\ \psi\uparrow$	$T\downarrow\ \psi\downarrow$
N_1	$\boldsymbol{v}_3$	$\boldsymbol{v}_5$	$\boldsymbol{v}_{11}$	$\boldsymbol{v}_9$
N_2	$\boldsymbol{v}_4$	$\boldsymbol{v}_6$	$\boldsymbol{v}_{12}$	$\boldsymbol{v}_{10}$
N_3	$\boldsymbol{v}_5$	$\boldsymbol{v}_7$	$\boldsymbol{v}_1$	$\boldsymbol{v}_{11}$
N_4	$\boldsymbol{v}_6$	$\boldsymbol{v}_8$	$\boldsymbol{v}_2$	$\boldsymbol{v}_{12}$
N_5	$\boldsymbol{v}_7$	$\boldsymbol{v}_9$	$\boldsymbol{v}_3$	$\boldsymbol{v}_1$
N_6	$\boldsymbol{v}_8$	$\boldsymbol{v}_{10}$	$\boldsymbol{v}_4$	$\boldsymbol{v}_2$
N_7	$\boldsymbol{v}_9$	$\boldsymbol{v}_{11}$	$\boldsymbol{v}_5$	$\boldsymbol{v}_3$
N_8	$\boldsymbol{v}_{10}$	$\boldsymbol{v}_{12}$	$\boldsymbol{v}_6$	$\boldsymbol{v}_4$
N_9	$\boldsymbol{v}_{11}$	$\boldsymbol{v}_1$	$\boldsymbol{v}_7$	$\boldsymbol{v}_5$
N_{10}	$\boldsymbol{v}_{12}$	$\boldsymbol{v}_2$	$\boldsymbol{v}_8$	$\boldsymbol{v}_6$
N_{11}	$\boldsymbol{v}_1$	$\boldsymbol{v}_3$	$\boldsymbol{v}_9$	$\boldsymbol{v}_7$
N_{12}	$\boldsymbol{v}_2$	$\boldsymbol{v}_4$	$\boldsymbol{v}_{10}$	$\boldsymbol{v}_8$

torque error to further improve torque performance. The duration of the selected voltage vectors and $\boldsymbol{v}_0$, denoted as t_b and t_0, respectively, are given by

$$t_b = \begin{cases} 0.6T_s & \Delta T > 20, \Delta T < -20 \\ (0.3/20\Delta T + 0.3)T_s & 20 \geqslant \Delta T > 0 \\ (-0.3/20\Delta T + 0.3)T_s & -20 < \Delta T \leqslant 0 \end{cases} \tag{3}$$
$$t_0 = T_s - t_b, \Delta T = T_{ref} - T$$

where T_s is the switching period, T is the instantaneous torque, and T_{ref} is the reference torque. A longer duration of the basic voltage vectors, t_b, is adopted when the torque error is large to generate enough torque. Conversely, when the torque is close to the reference value, t_b will be short, and the duration of the voltage vectors with even subscripts is $2t_b$ to accelerate the decreasing speed of the positive torque at the torque commutation zones.

4 Results of simulation and RT-LAB

To confirm the validity of the vector control method with the T-type three-level converter presented in this study, the results of the simulation and RT-LAB based on a three-phase 12/8 SRM are given in this section. The parameters of the SRM are shown in Tab. 4.

The simulation results are shown in Fig. 6, which as the same conditions as the simulation shown in Fig. 3 (i.e., reference speed of 500 r/min, reference torque of 60 N·m, reference flux linkage of 0.38 Wb). Comparing the three-phase torques of the two simulation results clearly shows that the negative torque in Fig. 6 decreases faster than the one in Fig. 3. Owing to the influence of the even subscript voltage vectors, the decreasing speed of the negative torque becomes equal to the increasing speed of the positive torque in the torque commutation zones.

The results of the RT-LAB are shown in Fig. 7 to Fig. 9, and consist of the total torque and three-phase currents. Under the same conditions as the simulation mentioned above, Fig. 7 shows that the results of the conventional control strategy based on six voltage vectors with a 117% torque ripple, and Fig. 8 shows the results based on the proposed 12 voltage vectors with a 20% torque ripple. From the aforementioned results, it is clear that the proposed method can solve the problem of torque ripple in the conventional DTC method. The RT-LAB results of the 12 vectors based on the proposed method at 1 000 r/min are depicted in Fig. 9. The total torque continues to be straight line, and the torque ripple is 13%.

Tab. 4 Parameters of the SRM

Parameter	Value
Phase nunber	3
Rated power/kW	25
Peak power/kW	60
Rated voltage/V	336
Rated speed/(r/min)	3 000
Number of stator/rotor poles	12/8

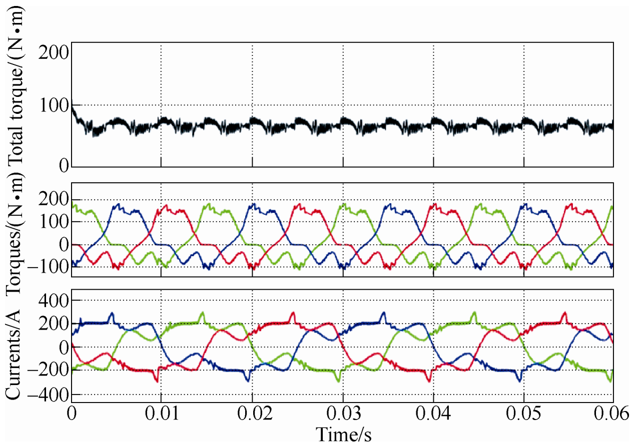

Fig. 6 Simulation results of twelve vectors based on the proposed method at 500 r/min

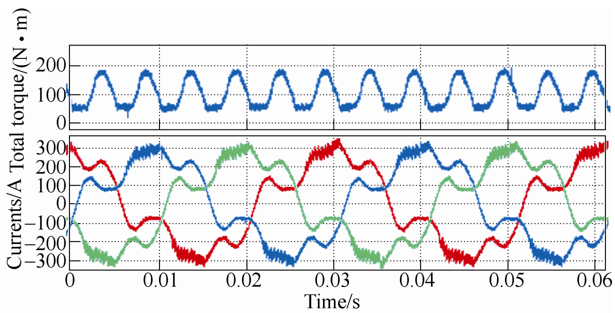

Fig. 7 RT-LAB results of six odd subscript vectors based on conventional DTC theory at 500 r/min

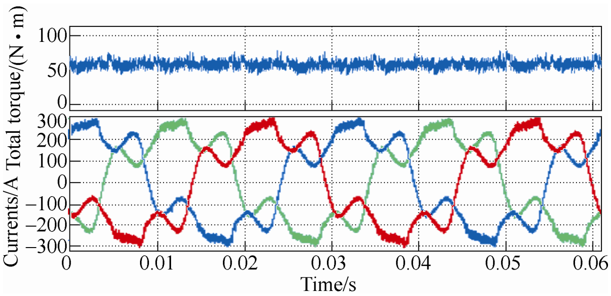

Fig. 8 RT-LAB results of 12 vectors based on the proposed method at 500 r/min

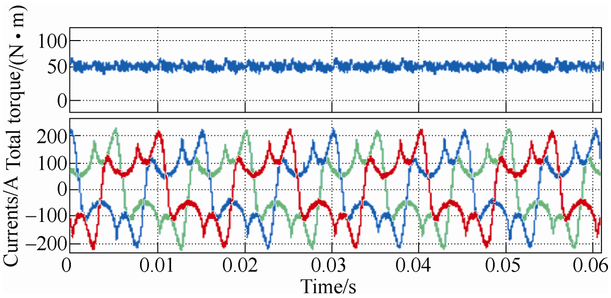

Fig. 9 RT-LAB results of twelve vectors based on the proposed method at 1 000 r/min

5 Conclusions

In this paper, a T-type three-phase converter was used to drive a switched reluctance motor, and a modified control strategy based on 12 voltage vectors was proposed to reduce the torque ripple, which the conventional six voltage vectors fail to achieve. The causes of torque ripple in the conventional six voltage vectors are analyzed. Subsequently, a zero-voltage vector is used to adjust the duration of the other vectors, and the time is varied at different parts of the voltage vector sectors. In addition, the delta connected windings can reduce the number of connections between the converter and SRM. Finally, the results of the MATLAB/Simulink and RT-LAB are used to validate the proposed scheme.

References

[1] J S Turner. New directions in communications. *IEEE J. Sel. Areas Commun.*, 1995, 13(1): 11-23.

[2] C R Neuhaus, N H Fuengwarodsakul, R W De Doncker. Predictive PWM-based direct instantaneous torque control of switched reluctance drives. *2006 37th IEEE Power Electronics Specialists Conference*, Jeju, 2006: 1-7.

[3] D Xuanju, X Peng, Y Haoming, et al. Phase plane-based variable structure control for switched reluctance motor direct torque control. *2012 12th International Conference on Control Automation Robotics & Vision* (*ICARCV*), Guangzhou, 2012: 775-781.

[4] N Yan, X Cao, Z Deng. Direct torque control for switched reluctance motor to obtain high torque–ampere ratio. *IEEE Transactions on Industrial Electronics*, 2019, 66(7): 5144-5152.

[5] H Abdelghani, A B Ben Abdelghani, I Slama-Belkhodja. Three level fault tolerant DTC control for induction machine drives. *International Multi-Conference on Systems, Signals & Devices*, Chemnitz, 2012: 1-6.

[6] M Elamin, Y Yasa, A Elrayyah, et al. Performance improvement of the delta-connected SRM driven by a standard three phase inverter. *2017 IEEE International Electric Machines and Drives Conference* (*IEMDC*), Miami, FL, 2017: 1-7.

[7] X Ai-de, Z Xianchao, H Kunlun, et al. Torque-ripple reduction of SRM using optimised voltage vector in DTC. *IET Electrical Systems in Transportation*, 2018, 8(1): 35-43.

[8] X Zhao, A Xu, W Zhang. Research on DTC system with variable flux for switched reluctance motor. *CES Transactions on Electrical Machines and Systems*, 2017, 1(2): 199-206.

[9] S Sau, R Vandana, B G Fernandes. A new direct torque control method for switched reluctance motor with high torque/ampere. *IECON 2013 - 39th Annual Conference of the IEEE Industrial Electronics Society*, Vienna, 2013: 2518-2523.

[10] W Ding, Y Hu, L Wu. Comparative evaluation of voltage space vector control and direct instantaneous torque control for switched reluctance motor drives. *2014 17th International Conference on Electrical Machines and Systems* (*ICEMS*), Hangzhou, 2014: 1808-1812.

[11] D Xuanju, X Peng, Y Haoming, et al. Phase plane-based variable structure control for switched reluctance motor direct torque control. *2012 12th International Conference on Control Automation Robotics & Vision* (*ICARCV*), Guangzhou, 2012: 775-781.

[12] M Abassi, A Khlaief, O Saadaoui, et al. Performance analysis of PMSM DTC drives under inverter fault. *2017 International Conference on Advanced Systems and Electric Technologies* (*IC_ASET*), Hammamet, 2017: 244-249.

[13] O M Abassi, I Saadaoui, A Tlili, et al. PMSM DTC drive system fed by fault-tolerant inverter connected to a photovoltaic source. *2018 9th International Renewable Energy Congress* (*IREC*), Hammamet, 2018: 1-5.

[14] J Zhang, L Li, D Dorrell, et al. Direct torque control with a modified switching table for a direct matrix converter

based AC motor drive system. *2017 20th International Conference on Electrical Machines and Systems* (*ICEMS*), Sydney, NSW, 2017: 1-6.

[15] A Ghaderi, M Sugai, T Umeno, et al. A new direct torque control for AC motors with over modulation ability. *2011 IEEE International Electric Machines & Drives Conference* (*IEMDC*), Niagara Falls, ON, 2011: 1247-1252.

Mingyao Ma received the B.S. and Ph.D. degrees in applied power electronics and electrical engineering from Zhejiang University, Hangzhou, China, in 2004 and 2010, respectively. From October 2008 to October 2009, she was a visiting PhD postgraduate research student in the University of Strathclyde, Glasgow, UK, and in 2010, she joined Zhejiang University as a Post-Doctoral Research Fellow. In 2011, she worked for the University of Central Florida, Orlando, US, as the visiting scholar. From April 2012 to April 2015, she joined the Newcastle University, Newcastle, UK, as the Research Associate. From 2015, she works in Hefei University of Technology as a professor. Her research interests include fault diagnostic technology for PV generation system, SR motor control, and health monitoring of power electronics systems.

Zhuangzhi Wang was born in Shanxi, China, in 1995. He received the B.S. degree in electrical engineering in 2017 from the School of Electrical Engineering and Automation, Hefei University of Technology, Hefei, China, where he is currently working toward the Master's degree in power electronics and power drives. His current research interests include vector control, control of conventional converters and advanced control method of switched reluctance motors and drives.

Qingqing Yang was born in Anhui, China, in 1990. She received the B.S. degree in electrical engineering in 2014 from the School of Electrical Engineering and Automation, Hefei University of Technology, Hefei, China, where she is currently working toward the Ph.D. degree in power electronics and power drives. Her current research interests include system analysis and design, parameters identification, and advanced control method of switched reluctance motors and drives.

Shuying Yang was born in Anhui, China, in 1980. He received the B.S. and Ph.D. degrees in electrical engineering from Hefei University of Technology (HFUT), Hefei, China, in 2002 and 2008, respectively. In 2005, he joined the teaching faculty of the School of Electrical Engineering and Automation, HFUT, where he is currently a Professor. From August 2014 to October 2015, he was a Visiting Scholar in the Department of Electrical and Computer Engineering, University of New Brunswick, Canada. His research interests include the wind power generation system, electrical drive, and grid-tied converters.

Xing Zhang was born in Shanghai, China, in 1963. He received the B.S., M.S., and Ph.D. degrees in electrical engineering and automation from Hefei University of Technology, Hefei, China, in 1984, 1990, and 2003, respectively. Since 1984, he has been a Faculty Member in the School of Electric Engineering and Automation, Hefei University of Technology, where he is currently a Professor. He also works in the Photovoltaic Engineering Research Center of the Ministry of Education. His main research interests include photovoltaic generation technologies, wind power generation technologies, and distributed generation systems.